One-Pot Large-Scale Synthesis of Robust Ultrafine Silica-Hybridized CdTe Quantum Dots

Li Zhou,[†,‡] Chao Gao,*[,‡] Xiaozhen Hu,[‡] and Weijian Xu*[,†]

Institute of Polymer Science and Engineering, College of Chemistry and Chemical Engineering, Hunan University, Changsha 410082, P. R. China, and MOE Key Laboratory of Macromolecular Synthesis and Functionalization, Department of Polymer Science and Engineering, Zhejiang University, 38 Zheda Road, Hangzhou 310027, P. R. China

ABSTRACT A facile one-pot strategy for synthesis of silica-hybridized CdTe quantum dots (SiO_2-*h*-CdTe QDs) in aqueous solution is presented, and subkilogram scale fluorescent SiO_2-*h*-QDs can be readily produced in one batch. This approach also makes the tuning of emission wavelength and absorption bandgap of SiO_2-*h*-QDs accessible for the first time. In the case of using MPA as ligand, the emission wavelength and absorption bandgap can be tuned in the range of 546−584 nm (the corresponding diameter of QDs increased from 2.0 to 3.2 nm) and 2.55−2.27 eV, respectively. The content of QDs in the resulting nanohybrids can also be readily adjusted in a wide range of 2−95 wt % by the feed ratio of QDs to silica precursors. The resulting SiO_2-*h*-QDs are ultrafine with diameters 8−16 nm, and show excellent optical properties, high stability, low toxicity, and versatile surface functionality compared with the neat QDs. Various functional groups such as amino, epoxy, and hydroxyl can be readily introduced to the surface of SiO_2-*h*-QDs by silane-coupling chemistry and surface-initiated polymerization. Our strategy opens up enormous opportunities to make full use of these robust fluorescent nanohybrids in various applications because of their facile availability, cost-effective productivity, and high stability.

KEYWORDS: quantum dots • silica • nanohybrids • fluorescent • large-scale

INTRODUCTION

Semiconductor quantum dots (QDs) have attracted increasing attention within recent years due to their promising applications in optical devices, solar cells, biosensors, and biological imaging (1−5). Because the surfaces of QDs are generally susceptible to external environment (6, 7), it is essential to endow the QDs surface with a protecting shell such as silica that has been widely used to protect inorganic nanoparticles such as iron oxide, gold, silver, and so on (8−14). Silica, not only providing chemical and physical shielding from the direct environment but also possessing good water dispersibility, biocompatibility, and surface functionality, is one of the most popular inert materials for surface protection (15−20).

Up to now, SiO_2-modified QDs have generally been prepared through two strategies: Stöber method (21−24) and reverse microemulsion method (25−31). The Stöber method involves first preparing hydrophilic QDs, and then the QDs act as seeds for the growth of silica shell in the mixture of ethanol and water. The second method was performed in a water-in-oil (W/O) reverse microemulsion system and the hydrolysis and condensation of the silica precursor occurs at the W/O interface or in the water phase, resulting in monodisperse silica particles. Both of the above two approaches could be used to produce core−shell QD@SiO_2 particles with single QD in the middle of silica and the diameter in the range of 25−150 nm, which exhibited much higher chemical and optical stability and biocompatibility than the neat QDs. However, all of the previous methods contain multistep complicated manipulations in which the QDs have to be presynthesized and separated before the SiO_2-coating reaction (Scheme 1A). Such tedious processes associated with very limited availability of products (usually less than 0.1 g at one time) and nontunability of bandgap seriously obstructed the practical applications of the modified QDs. In addition, the size of the reported QD@SiO_2 is generally too large (>30 nm), which would adversely affect their aqueous-solubility, dispersibility and processability, and thereby bionanoapplications. Therefore, exploring a facile strategy to large-scale synthesis of QD/SiO_2 nanohybrids with excellent optical stability, aqueous-solubility, and biocompatibility is fairly exigent. Because the yield and size of the products by the previous approaches are seriously limited, we aim to design a facile protocol for large-scale synthesis of ultrafine QD/SiO_2 nanohybrids and keep the comparable optical properties and biocompatibility to the conventional core−shell QD@SiO_2 at the same time.

Herein, we present a one-pot hybridization strategy to prepare SiO_2-hybridized CdTe QDs (SiO_2-*h*-QDs) up to subkilogram scale in one batch in lab. This approach was carried out in a sustainable water condition based on the first aqueous formation of CdTe QDs seeds followed by silica hybridization in the presence of tetraethyl orthosilicate

* To whom correspondence should be addressed. E-mail: chaogao@zju.edu.cn (C.G.); and weijxu@hnu.cn (W.J.X.).
Received for review January 18, 2010 and accepted March 10, 2010
† Hunan University.
‡ Zhejiang University.
DOI: 10.1021/am9009296

Scheme 1. (A) Conventional Multistep Approach for Synthesis of Core−Shell CdTe@SiO_2 Nanoparticles in Aqueous Solution or Microemulsion System via at Least Two Pots; (B) Presented One-Pot Strategy for Synthesis of SiO_2-Hybridized QDs in Aqueous Solution

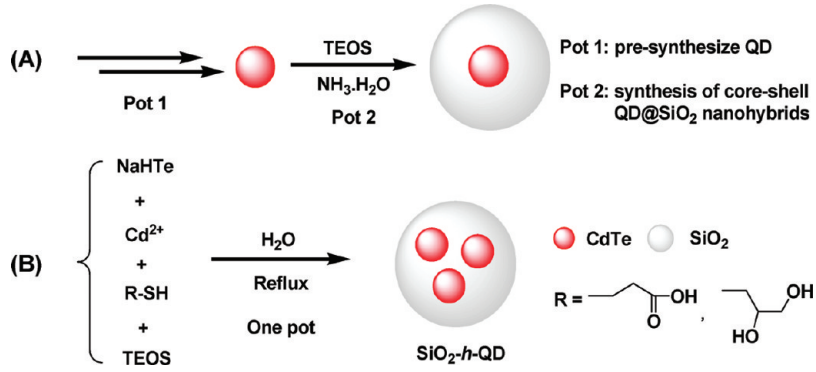

(TEOS) in the same reactor (Scheme 1B). Our strategy possesses various advantages: (1) the growth of QDs and silica-hybridization are performed in the same reactor by one step, which makes the synthetic process facile and the yield of QD/SiO_2 nanohybrids high (>90%); (2) the whole reaction process was conducted in aqueous solution under relative low temperature, which makes the synthesis environment green and the products cost-effective; (3) the resulting hybrid nanoparticles are ultrafine (8−16 nm), and the content of QDs in the product can be readily controlled by the weight feed ratio of the TEOS to CdTe, and more significantly; (4) similar to the neat QDs, the fluorescence emission wavelength and absorption bandgap of the nanohybrids can also be tuned by reaction time; (5) the as-prepared nanohybrids show excellent optical and chemical stability, and good biocompatibility and biostability compared with neat QDs due to the existence of the hybridized silica protecting; (6) the nanohybrids surface can be easily tailored with various functional groups through silane-coupling chemistry and surface-initiated polymerization for further modifications such as conjugation of drug molecules and grafting of desired polymers. It is expected that the facile and scalable synthesis of such robust ultrafine SiO_2-*h*-QD nanohybrids would pave the way for applying them in the classic fields such as bioimaging and immunoassay, and simultaneously arouse the new exploration of their applications such as in anticounterfeiting materials, high-performance quantum dots-polymer nanocomposites, and so on.

EXPERIMENTAL SECTION

Materials. Tellurium powder (Te, 99.8%), cadmium chloride ($CdCl_2$, 99+%), sodium borohydride ($NaBH_4$, 96%), 1-thioglycerol (TG, 90+%), glycidol (96%), mercaptopropionic acid (MPA, 99+%), tetraethyl orthoslicate (TEOS, 98%), 3-aminopropyltrimethoxysilane (APS, 97%), 3-glycidoxypropyltrimethoxysilane (GPS, 98%), and octadecyl isocyanate (90%) were purchased from Sigma-Aldrich and used as-received. Potassium methylate solution in methanol (CH_3OK, 25%) was obtained from Alfa Aesar and used as received. Dioxane and tetrahydrofuran (THF) were freshly distilled in the presence of calcium hydride before each polymerization. All other reagents used are of analytical grades without further purification.

Synthesis of SiO_2-*h*-CdTe Nanohybrids. Water-soluble SiO_2-*h*-CdTe nanohybrids were prepared by a one-pot approach. In a typical procedure, 560 mg of $NaBH_4$ was transferred to a small flask, and then 5.0 mL of ultrapure water was added. After 750 mg (5.9 mmol) of tellurium powder was added, the reacting flask was cooled by ice. During the reaction, a small outlet connected to the flask was kept open to discharge the pressure from the resulting hydrogen. After several hours, the black tellurium powder disappeared and white sodium tetraborate precipitate appeared on the bottom of the flask instead. The resulting fresh oxygen-free NaHTe aqueous solution was added to 2.0 L of N_2-saturated $CdCl_2$ solution (3.6 mM) at pH 9.0 adjusted by NaOH (1.0 M) in the presence of TG (2.68 g, 24.8 mmol) at 100 °C. After 10 min, 32.6 mL of TEOS was injected into the mixture. The mixture was then refluxed for 10 h before the CdTe QD/silica nanohybrids were precipitated by ethanol. The supernatant was discarded, and the nanohybrids were centrifuged and washed with ethanol repeatedly. After purification, the resulting orange solid was dried at 60 °C for 24 h under a vacuum, obtaining 10.05 g of SiO_2-*h*-CdTe nanohybrids (quantum yields: 15%).

The theoretical mass percentage of CdTe QD in the SiO_2/QD hybrids is defined as W_{theo} ($W_{theo} = QD_{mass}/(QD_{mass}+SiO_{2mass})$, where QD_{mass} is the mass of QDs that was predetermined by a control experiment without the addition of TEOS, and SiO_{2mass} is the mass of silica calculated from the feed mass of TEOS).

For preparation of SiO_2-*h*-CdTe nanohybrids at very low W_{theo} (e.g., 2.1 wt %) or at high pH (e.g., 10), a tiny mass (<1 wt %) of pure silica spheres would be formed. The pure silica can be easily separated by direct centrifugation because of their relative big size (25−35 nm). We also did several larger-scale batchs of experiments in 5 L flask with the same protocol described above, and 80−200 g of products with the same quality (Quantum Yields: 8%−16%) could be obtained in one-batch. The size of the larger-scale batches products also depended on the W_{theo} and in the range of 8−16 nm.

Control Experiment in the Presence of Ammonia. Typically, 0.5 mL of fresh-prepared NaHTe aqueous solution was injected to 200 mL of N_2-saturated $CdCl_2$ solution (3.6 mM) at pH 9.0 adjusted by ammonia (25 wt %) in the presence of TG (270 mg, 2.48 mmol) at 100 °C. After 10 min, 2 mL of TEOS was added into the mixture. The mixture was then stirred and refluxed. With the increase in time, the mixture became more and more cloudy. Finally, a thick white solid layer appeared at the bottom of the mixture. The solids were collected by direct centrifugation and then washed by deionized water. After three cycles of washing-centrifugation, the resulting white solids (SiO_2) were dried under a vacuum at 80 °C for 24 h. By analyzing the weight of the obtained dried SiO_2, we found that almost all of the TEOS were transformed into pure silica. This indicates that SiO_2 did not hybridize on the QDs surface but only simply blend the QDs in solution.

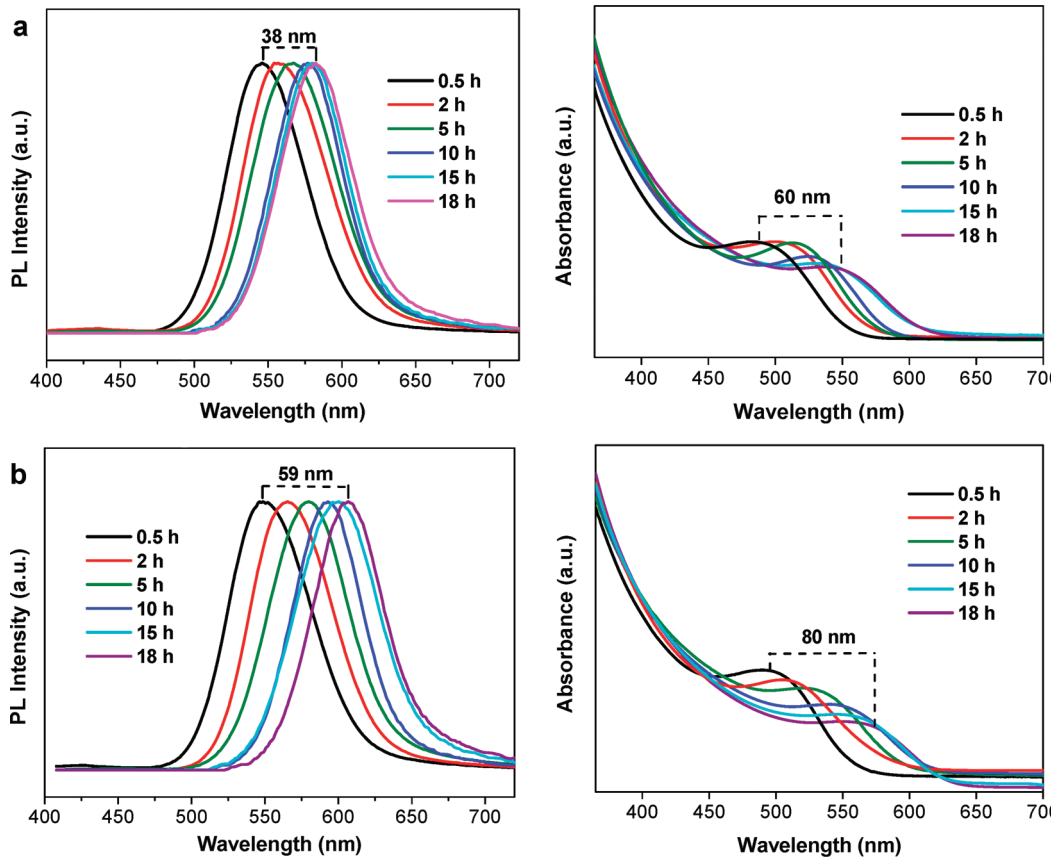

FIGURE 1. Emission (left) and absorption (right) spectra of (a) SiO_2-hybridized CdTe QDs and (b) neat CdTe QDs prepared in aqueous solution using MPA as ligand at different reaction times.

Functionalization of SiO_2-*h*-CdTe through Silane-Coupling Chemistry. SiO_2-*h*-CdTe nanohybrids with different surface functional groups can be readily fulfilled by silane-coupling chemistry. Typically, into a 100 mL flask were charged 100 mg of SiO_2-*h*-CdTe, 0.5 mL of APS (2.86 mmol) and 50 mL of toluene, and the mixture was then stirred at 95 °C for 6 h. The product was separated by centrifugation and washed with ethanol repeatedly. The product of amino-CdTe/SiO_2 nanohybrids can still be well-dissolved in water. After the further reaction with octadecyl isocyanate at 50 °C for 4 h, the obtained hydrophobic SiO_2-*h*-CdTe can be dissolved in organic solvents such as chloroform, and *N*,*N*-dimethylformamide (DMF), et al. In addition, the SiO_2-*h*-CdTe nanohybrids obtained from the larger-scale batchs have the same chemical robustness.

Synthesis of Hyperbranched Polyglycerol (HPG)-Grafted SiO_2-*h*-CdTe (32). Typically, SiO_2-*h*-CdTe nanohybrids (50 mg) were mixed with 28 μL (0.47 mmol) of potassium methylate (CH_3OK) solution and 2.0 mL of anhydrous tetrahydrofuran (THF) in a flask. The mixture was stirred for 1 h, before which excess methanol was removed by vacuum. Then, 8.0 mL of anhydrous dioxane was added and the flask was kept in an oil bath at 95 °C. Glycidol (1.0 g, 13.5 mmol) was added dropwise over a period of 10 h. After completion of monomer addition the mixture was stirred for an additional 1 h. The mixture was quenched and dispersed in methanol, and subsequently separated by centrifugation and washed with methanol. After repeated washing/separation steps and drying overnight in a vacuum, the HPG-attached nanohybrids (SiO_2-*h*-CdTe@HPG) was obtained.

Characterization. Thermal gravimetric analysis (TGA) was carried on a PE TGA-7 instrument with a heating rate of 20 °C min^{-1} in a nitrogen flow (20 mL min^{-1}). Fourier transform infrared (FTIR) spectra were recorded using a PE Paragon 1000 spectrometer (KBr disk). UV−vis spectra were recorded on a PE Lambda 20/2.0 UV/vis spectrometer. Emission spectra were collected using a Varian Cary 100 spectrometer. X-ray powder diffraction (XRD) spectra were taken on a Bruker AXS D8-advance X-ray diffractometer with Cu Kα radiation. X-ray photoelectron spectroscopy (XPS) was investigated on a RBD upgraded PHI-5000C ESCA system (Perkin-Elmer) with Mg Kα radiation ($h\nu$ = 1253.6 eV), binding energies calibration was based on C1s at 284.6 eV. Transmission electron microscopy (TEM) studies were performed on a JEOL JEL2010 electron microscope at 200 kV. Fluorescence images were obtained with Zeiss LSM-510 confocal laser-scanning microscope using a laser at 405 nm. The dynamic light scattering (DLS) measurements were conducted using a Brookhaven particle size and zeta potential analyzer at room temperature.

RESULTS AND DISCUSSION

One-Pot Synthesis of SiO_2-*h*-CdTe Nanohybrids with Tunable Optical Properties. The one-pot scalable-synthesis process of SiO_2-*h*-CdTe is similar to the corresponding neat CdTe in aqueous solution by using thiol-molecules such as 3-mercaptopropionic acid (MPA) and 1-thioglycerol (TG) as ligands (Scheme 1B) (33−35). The only difference lies in the addition of TEOS after the NaHTe precursor was injected into the mixture for 10 min, when the primary CdTe QDs (or QD seeds) were formed. The whole reaction process was monitored by photoluminescence (PL) and absorption spectra as shown in Figure 1. In the cases of MPA as ligand, the PL peak first shifted from 546 to 576 nm in 10 h and subsequently from 576 to 584 nm for another 8 h, and similarly, the corresponding absorption peak shifted from 488 nm (2.55 eV) to 532 nm

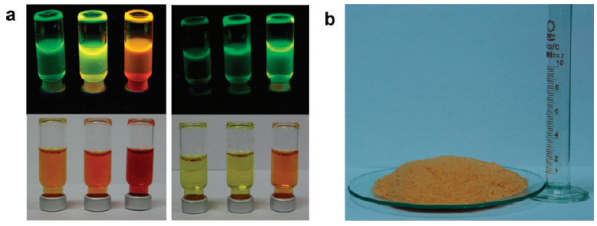

FIGURE 2. (a) Photographs of SiO_2-hybridized CdTe QDs in aqueous solution under UV light (365 nm, top) and daylight (bottom), confirming their high water solubility and tunable optical properties. The left three samples were prepared with MPA as ligand (from left to right the reaction time is 0.5, 5, and 18 h, respectively) and the right three samples with TG as ligand (from left to right the reaction time is 1, 7, and 31 h, respectively). (b) Photograph of SiO_2-hybridized CdTe QDs powder obtained in one batch.

(2.34 eV) in the first 10 h and from 532 nm (2.34 eV) to 548 nm (2.27 eV) for another 8 h, suggesting that the luminescence color and bandgap can be tuned by the reaction time to some extent (Figure 1a). These results also indicate that the in situ formed SiO_2-*h*-CdTe nanohybrids have the size-dependent quantum confinement effect that is one of the most important natures of conventional QDs. By comparison, both of the PL and absorption peaks of neat CdTe QDs showed gradually red shift during the reaction process even after 18 h (Figure 1b). The shifted wavelength range in emission spectra is 38 nm for SiO_2-*h*-CdTe and 59 nm for neat CdTe QDs, and correspondingly in absorption spectra is 60 nm for SiO_2-*h*-CdTe and 80 nm for neat CdTe QDs in 18 h by using MPA as ligand. According to the empirical fitting functions proposed by Peng and co-workers (36), the diameter of the CdTe nanocrystals in the SiO_2-*h*-CdTe nanohybrids based on the first excitonic absorption peak is calculated to be 2.0, 3.0, and 3.2 nm at reaction times of 0.5, 10, and 18 h, respectively. In comparison, the diameter of neat CdTe nanocrystals without addition of TEOS is calculated to be 2.2, 3.3, and 3.5 nm at reaction times of 0.5, 10, and 18 h, respectively, which is slightly bigger than in SiO_2-*h*-CdTe nanohybrids at the same reaction time. This suggests that QDs grow more slowly in the presence of TEOS because of their hybridization reaction.

Similar shifting phenomena can also be observed in the cases of using TG as ligand. The shifted wavelength range is 21 nm for SiO_2-*h*-CdTe and 33 nm for neat CdTe QDs in 48 h in PL spectra, and is 45 nm for SiO_2-*h*-CdTe and 58 nm for neat CdTe QDs in 48 h in absorption spectra (see Figure S1 in the Supporting Information).

The as-prepared SiO_2-*h*-CdTe hybrids can be easily dissolved in water and exhibit strong fluorescence in aqueous solution under UV light (Figure 2a). In addition, different ligands can give birth to different emission wavelengths by keeping other parameters as constant, and for MPA ligand green-yellow, yellow, and red luminescence (emission peak from 546 to 584 nm) while for TG ligand green and green-yellow luminescence (emission peak from 515 to 536 nm) can be observed under UV light (Figure 2a). The different emission wavelength ranges for MPA and TG are likely derived from the differences of the molecular structure and terminal functional groups of the ligands as reported by Zhang et al in the synthesis of neat CdTe quantum dots (34).

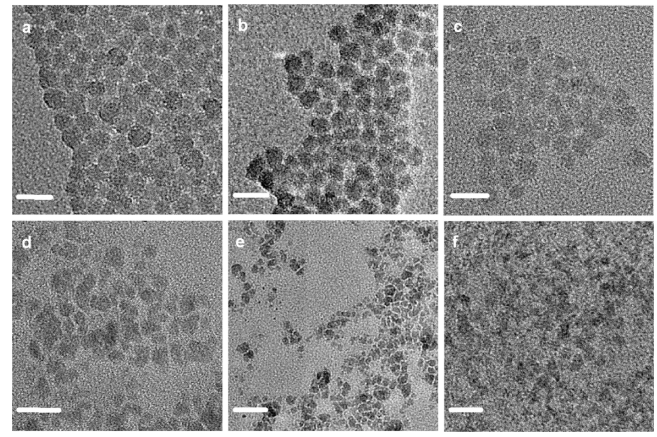

FIGURE 3. TEM images of SiO_2-hybridized CdTe QDs with W_{theo} (a) 2.1, (b) 9.4, (c) 19.7, (d) 32.5, (e) 48.6, and (f) 84.9 wt %. All the scale bars are 20 nm.

The MPA has a thiol group and a carboxylic group, whereas TG has a thiol group and two hydroxyl groups. The thiol group directly caps on the QDs, whereas the other terminal functional group is exposed to the surrounding and may affect the coalescence and fusion of ionic monomers and clusters. In the same reaction condition, the carboxylic groups of MPA may coordinate with the Cd site of monomers or clusters, leading to fast growth of CdTe crystal. For TG, the two terminal hydroxyl groups have very weak interaction with Cd site monomers or clusters and moreover have bigger steric hindrance for the coalescence of their capped monomers or clusters, thus result in very slow crystal growth. To the best of our knowledge, this is the first example to directly synthesize SiO_2-*h*-CdTe nanohybrids with tunable luminescence color. Moreover, subkilogram scale products can be readily obtained in one batch (Figure 2b) because of the high yield (~93%) of this methodology, implying the scalable productivity of the nanohybrids.

To further understand the reaction process and demonstrate the good reproducibility of our one-pot synthesis strategy, we designed and conducted a series of experiments with different feed ratios of CdTe to TEOS (or W_{theo}). With the variation of W_{theo} from 0 to 100 wt %, a series of products were prepared. The detailed characterizations are given below.

TEM Observations. The structure and morphology of the resulting SiO_2-*h*-CdTe materials were observed through transmission electron microscope (TEM) as shown in Figure 3. The SiO_2-*h*-CdTe particles are generally spherical shape and their size in the range of 8−16 nm, which would be beneficial to SiO_2-*h*-CdTe solubility and following bionanoapplications. We found that the size and morphology of the SiO_2/QD nanohybrids could be tuned to some extent by adjusting the TEOS concentration. When W_{theo} is higher than 19.7 wt %, with increasing the concentration of TEOS (or decreasing the W_{theo}) the hybrids morphology is closer to spherical shape and their sizes became more uniform and bigger (e.g., the average diameter of the samples with W_{theo} 48.6 and 32.5 wt % are 9 and 10 nm, respectively). When W_{theo} lower than 19.7 wt %, the concentration of TEOS has very slight influence on the hybrids morphology and size

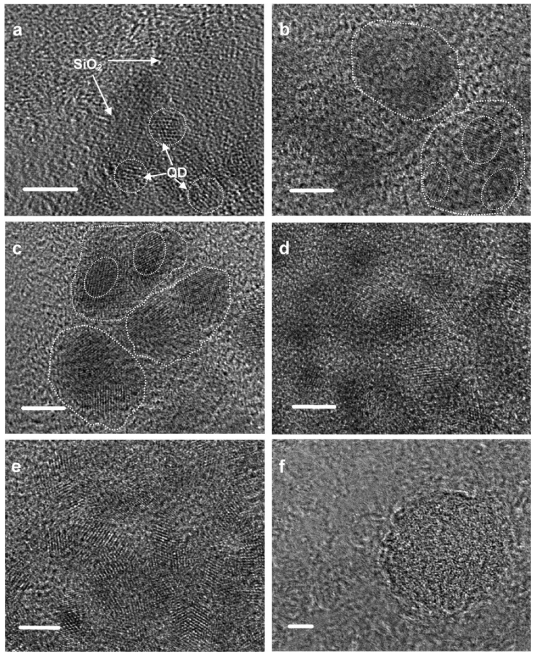

FIGURE 4. High-resolution TEM images of SiO_2-hybridized CdTe QDs with W_{theo} (a) 9.4, (b) 19.7, (c) 48.6, (d) 60.0, and (e) 84.9 wt %, and (f) pure SiO_2. The CdTe crystal lattice can be observed and was marked by a dash ring. The scale bar corresponds to 5 nm.

even for the sample with W_{theo} as low as 2.1 wt % (the corresponding silica content in the product is ca. 97.9 wt %). In addition, dynamic light scattering (DLS) was utilized to determine the hydrodynamic diameter of the SiO_2-*h*-CdTe particles with different W_{theo} in aqueous solution as shown in Figure S2. The diameters of the SiO_2-*h*-CdTe in aqueous solution are also very small (below 25 nm). Similar to the TEM results, with the decrease of W_{theo}, the size and size distribution of SiO_2-*h*-CdTe became bigger and more uniform from the DLS measurements, respectively. All these showed that ultrafine silica nanoparticles decorated with controllable and tiny amount of QDs can be easily fabricated, which is crucial for the industrial production and application of hybrid nanomaterials. High-resolution TEM (HRTEM) observations showed that our synthesized QD/SiO_2 particles are not in the form of single QD as core and silica as shell, but in the form of a hybrid in which QDs phase and silica phase are embedded each other (Figure 4a,b,c). So we coined our products as SiO_2-*h*-QDs instead of QD@SiO_2. The CdTe QDs are well-crystallized and their crystal lattice can be clearly observed under HRTEM. In addition, seen from the HRTEM images, the size of the CdTe QDs is slightly increased with the increase of W_{theo} to some extent (e.g., the average diameter of the QDs with W_{theo} 9.4 and 48.6 wt % are 3 and 4 nm, respectively). This may due to the samples with low W_{theo} possess thicker silica interlayer at the same reaction time and hence prevent or decrease the coalescence of Cd site monomers or cluster, leading to slow growth of CdTe crystal in the silica matrix. On the other hand, because of the low contrast, with the increase in W_{theo} the silica components in the HRTEM became more and more difficult to detect (Figure 4d,e).

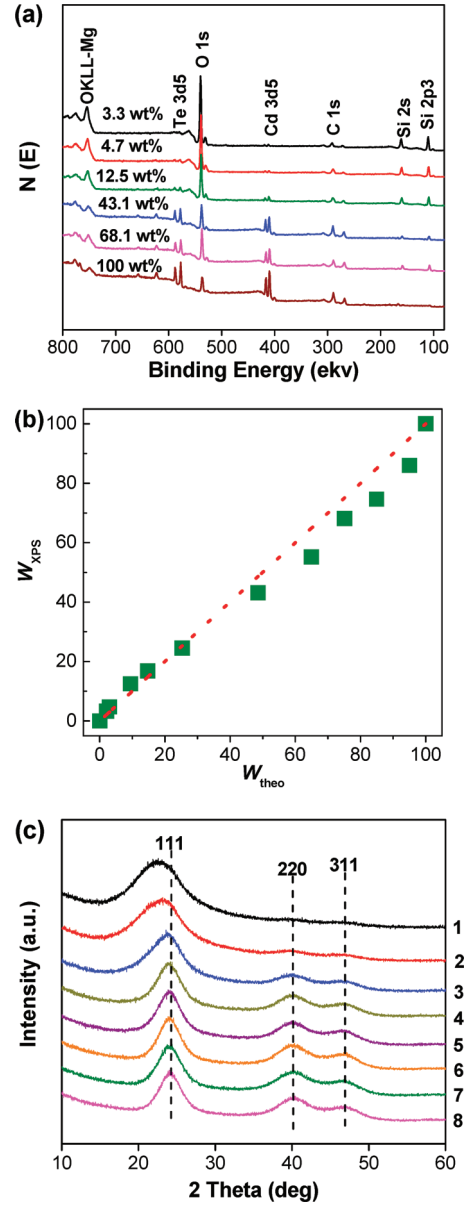

FIGURE 5. (a) Representative X-ray photoelectron (XPS) spectra of neat CdTe QDs and SiO_2-hybridized CdTe QDs with different W_{XPS}. (b) Relationship of calculated W_{theo} vs the determined W_{XPS} by XPS. (c) XRD patterns for SiO_2-hybridized CdTe QDs with W_{theo} (2) 2.1, (3) 9.4, (4) 32.5, (5) 48.6, (6) 60.0, and (7) 84.9 wt %, (1) pure SiO_2, and (8) neat CdTe QDs.

XPS and XRD Characterizations. For gaining more structure information of the as-prepared nanohybrids, the chemical composition was analyzed by X-ray photoelectron spectroscopy (XPS) (Figure 5a). According to the full survey spectrum, the elements of Cd, Te, Si, O, and C were found, of which the elements of Cd, and Te arise from the CdTe QDs, and the elements of C, O,and Si arise from SiO_2 and thiol-ligands. Meanwhile, the mass percentage of CdTe in the SiO_2-*h*-CdTe particles was also calculated according to the XPS results (W_{XPS}) with the content of Si element as reference. It is found that the W_{XPS} is very close to the W_{theo} in the wide range (0−100 wt %), suggesting that the content of QDs can be tuned with favorable controllability (Figure 5b). This result further demonstrates the advantage of our one-pot strategy.

Scheme 2. Speculated Growing Hybridization Mechanism for One-Pot Synthesis of SiO_2-Hybridized QDs

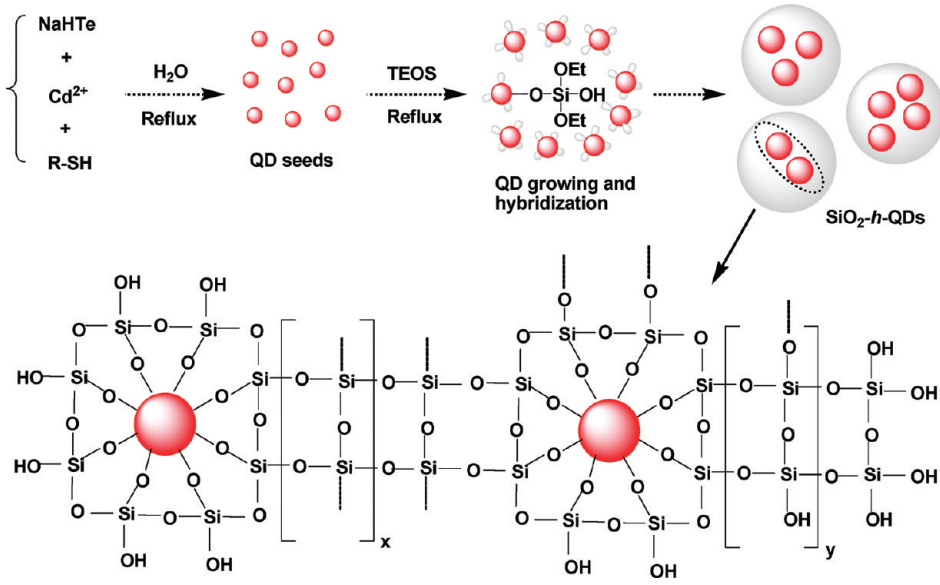

The crystalline structures of SiO_2-*h*-CdTe series products were determined by powder X-ray diffraction (XRD) (Figure 5c). The diffraction patterns of the peaks generally fit to the cubic zinc blende structure of bulk CdTe crystal, and the broad peak around 23° in the samples with CdTe weight content lower than 9.4 wt % is typically caused by the amorphous silica (34). In addition, as the W_{theo} decreases, the relative intensities of the peaks assigned to CdTe QDs become weaker because of the lower content of QDs and thicker silica interwalls.

It is noteworthy that the results mentioned above are highly reproducible in our tens of repeated experiments, further declaring the good controllability of the one-pot synthesis strategy. In addition, we found that the pH can play an important role on controlling the reaction speed, and the suited pH range is 8−10. At lower pH, the QD surface is not stable and thus shows low photoluminescence QYs, whereas at higher pH, silica may degrade after exposure in excess NaOH environment for long time.

Synthesis Mechanism Speculation. Though the accurate mechanism for the formation of SiO_2-*h*-CdTe is not completely known, we could speculate the possible hybridization mechanism according to the observed phenomena and obtained results. It is known that ammonia is commonly used in the literature as catalyst to accelerate the hydrolysis of TEOS, affording QD@SiO_2 and other silica structures (22, 37). To probe the mechanism of our strategy comparatively, we also performed the experiments in the presence of ammonia, whereas found that the silica could not hybridize with the CdTe QDs but self-nucleated to form pure SiO_2 spheres (see Figure S3 in the Supporting Information) (25, 26).

In our cases, because ammonia is not added, when TEOS was added to the reaction system, the hydrolysis of TEOS takes place very slow. The hydrolyzed TEOS would contact with and then adsorb onto the QD seeds because of the interactions of electrostatic force, hydrogen bonds, hydrophobic force, and so on. The condensation of adsorbed TEOS with the interface protic functional groups (e.g., −OH, −COOH) gives rise to QD-TEOS hybrid sol that gradually condenses into hybrid nanoparticles embedded with simultaneously aged QDs according to the similar formation procedure of pure silica NPs (Scheme 2). The condensation and cross-linking between QD-TEOS and TEOS is a very slow process, providing the chance and channels for the growth or aging of QDs. So the bandgap and QD size of nanohybrids can be tuned by the reaction time to some extent in experiments. In addition, the influence of the molecular structure and terminal functional groups of the ligand on the growth of the CdTe crystal associated with the emission wavelength range was also taken place in this process. With the increase of cross-linking degree, the channels become narrower and less, and hence the growth of enveloped QDs get more slowly until stop finally when the silica interlayer forms closely. This is in accordance with the aforementioned experimental phenomena and results.

To further understand the reaction mechanism, the reaction process was monitored by TEM and DLS. As shown in Figure 6, at the early reaction stage (Figure 6a,b), the morphology of the sample particles was irregular. According to the above speculated mechanism, this may due to that the hydrolysis of TEOS formed SiO_2 sol and the sol was not completely cross-linked. As prolonging the reaction time, the particles aggregated and tended to form spherical shape particles (Figure 6c). Finally, uniform spherical SiO_2-*h*-CdTe particles were formed (Figure 6d). From the DLS results (see Figure S4 in the Supporting Information), the size of the sample particles generally increased at beginning with the increase of reaction time and at 5 h exhibited the maximum diameter (D) and size polydispersity index (PDI) (D = 28.69 nm, PDI = 0.213). Nevertheless, further prolonged the reaction time, the size decreased to 22.38 nm with PDI = 0.113. Therefore, both the TEM and DLS results are well-consistent with the speculated reaction mechanism that the formation of SiO_2-*h*-CdTe nanohybrids included the slow

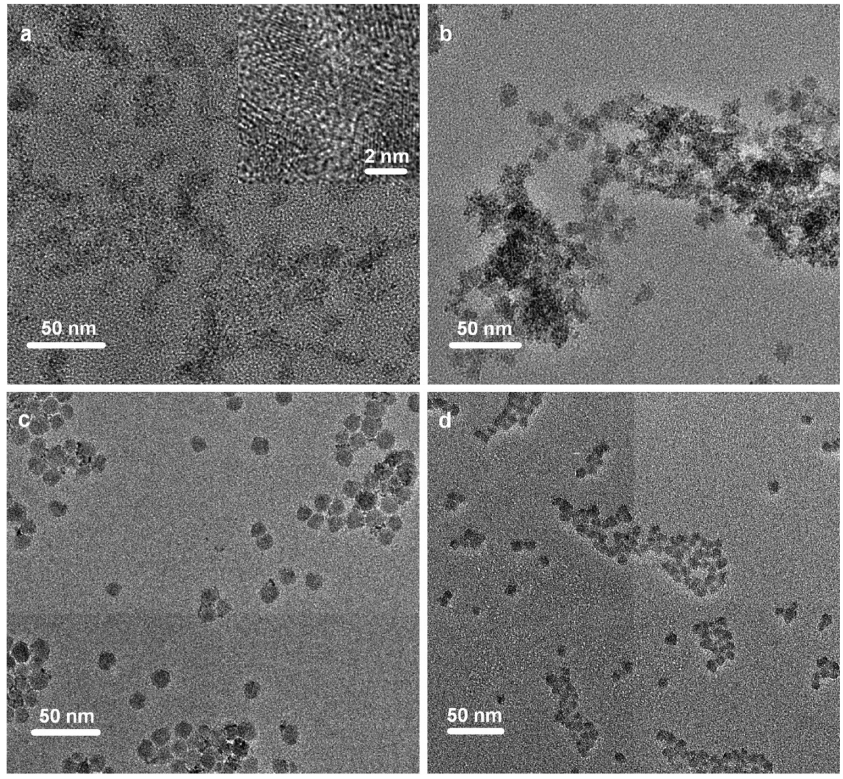

FIGURE 6. TEM images of SiO_2-hybridized CdTe sample with W_{theo} 19.7 wt % at the reaction time (a) 10 min, (b) 1 h, (c) 5 h, and (d) 18 h.

hydrolysis of TEOS to form SiO_2 sol and the gradual cross-link of the SiO_2 sol to form SiO_2-*h*-CdTe particles.

According to this mechanism, it is reasonable to speculate that pure SiO_2 spheres may be formed at very low W_{theo} because of the existence of possible competing reaction between the condensation of silica sol on CdTe surface and the self-condensation of silica sol to form pure SiO_2 spheres. In fact, a tiny mass of pure silica (<1 wt %) was observed for the case of W_{theo} 2.1 wt %. This result demonstrated the rationality of the mechanism, and also indicated the very low probability of silica sol self-nucleation in the presence of QDs. Nevertheless, to obtain highly pure SiO_2/CdTe nanohybrids, the formed pure silica can be easily removed by centrifugation because of their relative bigger size (25−30 nm). Because the hybridization (or hydrolysis of TEOS) and growth of QDs occur simultaneously, the formation mechanism of SiO_2-*h*-CdTe can be named as "growing hybridization". Such a dynamic process is essentially different from the conventional static ones in which the sizes of presynthesized QDs are unchanged and the bandgap of resulting products cannot be tuned yet.

Evaluations of Optical Stability, Biostability, and Toxicity of SiO_2-*h*-QDs. Because our synthesized SiO_2-*h*-QDs do not possess the structure with single QD in the middle of silica, it is crucial to know whether the optical properties, chemical and biological stabilities are comparable to the previously reported QDs@SiO_2 nanoparticles (26, 27). To our delight, the QYs of the as-prepared SiO_2-*h*-QDs with different CdTe contents are generally in the range of 15−19%, which are comparable to the values of the previously reported QDs@SiO_2 nanoparticles, and are higher than that of the neat QDs (15%) as shown in Figure 7a. This can be explained by the fact that the self-quenching effect of QDs, which is caused by the particles aggregation, can be effectively avoided because of the presence of silica isolation layer compared to neat QDs, especially for the sample with relatively high SiO_2 content (38). The photooxidation experiments were also performed under UV light by comparing the time ($T_{1/2}$) (Figure 7a), when the PL intensity of SiO_2-*h*-QDs decreases to its half initial. Generally, the SiO_2-*h*-QDs showed much higher $T_{1/2}$ compared to neat QDs, and more silica content resulted in longer $T_{1/2}$, because the silica hybridization could isolate the QDs from the environment effectively to avoid contacting oxygen and water directly. For instance, the $T_{1/2}$ for neat QDs is only 19 min, while for the SiO_2-*h*-QDs with silica content 50 wt % the $T_{1/2}$ rises to 44 min that is about 2.5 times of the neat QDs. The longest $T_{1/2}$ is 58.5 min with silica content 90 wt %, which is more than 3 times that of the neat QDs. In addition, with the silica content greater than 60 wt %, the $T_{1/2}$ increased slowly with the increase in silica content, suggesting that the QDs were almost totally enveloped by silica above this fraction.

Moreover, to confirm the SiO_2-*h*-QDs are more stable under bioenvironment compared to the neat QDs, the PL stabilities in phosphate buffer were also investigated at pH 6.8 and 8.5. As shown in Figure 7b, the PL intensity of neat QDs decreased sharply to ca. 18% after only 5 h, and was completely quenched within 24 h at pH 6.8, while for SiO_2-*h*-QDs with CdTe contents of 9.4 and 25.3 wt % both can still keep 90% of initial intensity after 24 h. At pH 8.5, the neat CdTe QDs only maintained ca. 30% of initial emission

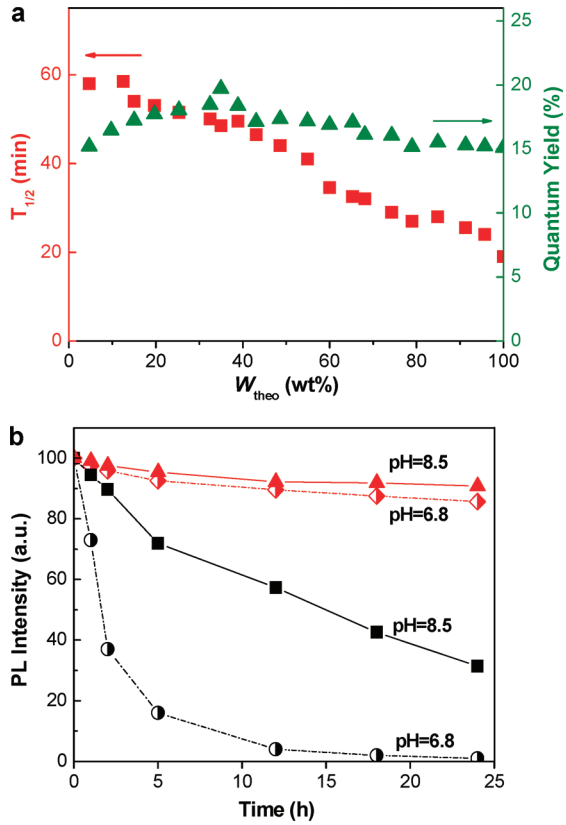

FIGURE 7. (a) Quantum yields of neat CdTe and SiO_2-hybridized CdTe QDs with different W_{theo}, and photostability of SiO_2-hybridized CdTe QDs with W_{theo} 9.4 wt % (3 mg/mL) under UV light (365 nm). (b) PL-stability of neat CdTe (black line) and SiO_2-hybridized CdTe QDs (red line) with W_{theo} 9.4 wt % in the phosphate buffer solution (3 mg/mL) at pH 6.8 and 8.5.

efficiency after 24 h, while the PL intensity of the SiO_2-*h*-QDs almost kept constant. These results demonstrate that our SiO_2-*h*-QDs are also highly stable in both acid and base buffer solutions, promising their potential applications in bionanotechnology.

Consequently, we studied the in vitro cell imaging with the SiO_2-*h*-QDs in the malignant melanoma cells A375, and strong green fluorescence could be detected in cells even after 8 h (see Figure S5b in the Supporting Information). On the contrary, the fluorescence was almost bleached in cells within 5 h for neat QDs (32). So the silica hybridization can significantly improve the biostability of QDs indeed. On the other hand, because the toxicity of QDs is a big challenge for bioapplications, in vitro cytotoxicity evaluations of SiO_2-*h*-QDs and neat CdTe QDs in human lung cancer cells SPCAI were conducted, and the results showed that the SiO_2-*h*-QDs were much less toxic than the neat QDs (see Figure S5a in the Supporting Information) (39). This is likely due to the silica shell can prevent the CdTe dissolution, which would result in the release of free Cd^{2+} and chalcogenoxides under oxygen and photoirradiation.

Therefore, it can be concluded that the SiO_2-*h*-QDs can not only be readily and scalablly prepared via the one-pot aqueous approach but also have excellent optical property, high water-solubility, photostability, chemical and biological stabilities, and biocompatibility.

Chemical Reactivity of SiO_2-*h*-QDs. To enhance the optical property, chemical stability, and biocompatibility of QDs, many inorganic matrices could be utilized to form hybrid structure such as CdTe/CdSe and CdTe/CdS (40, 41). However, their surface functional groups for further modification are not so convenient. For our SiO_2-*h*-QDs, another marked merit is their surface can be facilely modified through the classic silane-coupling chemistry (42, 43) and surface-initiated ring-opening polymerization, endowing various functional groups such as amino, epoxy, and hydroxyl for further functionalization (see Figure S6 in the Supporting Information), as verified by thermal gravimetric analysis (TGA) and Fourier transform infrared (FTIR) spectra (see Figure S7 in the Supporting Information). For unmodified SiO_2-*h*-QDs, only ca. 2 wt % of weight loss was found below 700 °C, whereas after the surface modification, ca. 7.8, 10.5, and 33.1 wt % of weight loss for amino-, epoxy-, and hyperbranched polyglycerol (HPG)-functionalized SiO_2-*h*-QDs were detected between 100−500 °C, respectively (see Figure S7a in the Supporting Information). In addition, from the FTIR spectra, after the modification, two obvious bands at 2816 and 2901 cm^{-1} associated with C−H stretching appeared (see Figure S7b in the Supporting Information). All these characterizations demonstrated the successful surface modification of the SiO_2-*h*-QDs.

Herein, to demonstrate the high reactivity of the surface functional groups, we chose amino-functionalized SiO_2-*h*-QDs (SiO_2-*h*-QDs-NH_2) to further react with octadecyl isocyanate at 50 °C for 4 h. After the reaction, the weight loss increased from 7.8 to 20.4 wt % between 100 and 500 °C. Meanwhile, from the FTIR spectra, an obvious band at 1551 associated with the amide II stretching appeared (see Figure S7b in the Supporting Information). This is in accordance with the predicted structure as shown in Figure S6 in the Supporting Information. Moreover, we found that the solubility of the SiO_2-*h*-QDs can be facilely tuned by change the surface functional groups (see Figure S7d in the Supporting Information). The unmodified SiO_2-*h*-QDs can only be dissolved in aqueous solution and would be precipitated immediately in ethanol but the amino-, epoxy-, and HPG-functionalized SiO_2-*h*-QDs can be well dispersed in various organic solvents such as ethanol, tetrahydrofuran, and DMF. The SiO_2-*h*-QDs-C18 can even be well-dissolved in nonpolar organic solvents such as chloroform and dichloromethane because of the surface modification by the nonpolar organic moieties. More significantly, benefiting from the silica interlayer protection, no obvious decrease of photoluminescence QY for the hybrid QDs was observed during the chemical reactions (Note: the fluorescence of neat QDs might be quenched in 30 min during a common reaction such as esterification; see Figure S7c in the Supporting Information). Therefore, we can conclude that our synthesized SiO_2-*h*-QDs can be easily tailored with various highly reactive functional groups that can be utilized to conjugate functional molecules, and can keep excellent optical properties at the same time. This is extremely important for practical applications such as in bioimaging and biosensors.

CONCLUSION

In conclusion, we have reported a one-pot approach for large-scale preparation of silica-hybridized CdTe quantum dots with excellent controllability and high reproducibility. The as-prepared water-soluble SiO_2-*h*-QDs are ultrafine with an average diameter below 16 nm and show excellent optical stability, favorable biocompatibility, low toxicity, and facile surface functionality compared to the neat CdTe QDs. Meanwhile, their emission and absorption wavelengths can be tuned by the reaction time because of the growing hybridization mechanism. We believe that the work presented here will provide a significant step forward to bringing QDs from experiment research to practical applications such as optical devices fabrication, bioimaging, and multifunctional nanocomposites.

Acknowledgment. This work was financially supported by the National Natural Science Foundation of China (50773038 and 20974093), National Basic Research Program of China (973 Program) (2007CB936000), Science Foundation of Chinese University, and the Foundation for the Author of National Excellent Doctoral Dissertation of China (200527).

Supporting Information Available: QY measurements, optical spectra of SiO_2-*h*-CdTe using TG as ligand at different reaction time, photograph of the final mixture that was prepared in the presence of ammonia, dynamic light scattering (DLS) results of SiO_2-*h*-CdTe with different W_{theo} and reaction time, and biological evaluation and surface functionalization of the SiO_2-*h*-CdTe (PDF). This material is available free of charge via the Internet at http://pubs.acs.org.

REFERENCES AND NOTES

(1) Alivisatos, A. P. *Science* **1996**, *271*, 933–937.
(2) Kroutvar, M.; Ducommun, Y.; Heiss, D.; Bichler, M.; Schuh, D.; Abstreiter, G.; Finley, J. J. *Nature* **2004**, *432*, 81–84.
(3) Robel, I.; Subramanian, V.; Kuno, M.; Kamat, P. V. *J. Am. Chem. Soc.* **2006**, *128*, 2385–2393.
(4) Michalet, X.; Pinaud, F. F.; Bentolila, L. A.; Tsay, J. M.; Doose, S.; Li, J. J.; Sundaresan, G.; Wu, A. M.; Gambhir, S. S.; Weiss, S. *Science* **2005**, *307*, 538–544.
(5) Gao, X. H.; Cui, Y. Y.; Levenson, R. M.; Chung, L. W. K.; Nie, S. M. *Nat. Biotechnol.* **2004**, *22*, 969–976.
(6) Derfus, A. M.; Chan, W. C. W.; Bhatia, S. N. *Nano Lett.* **2004**, *4*, 11–18.
(7) Zhang, T.; Stilwell, J. L.; Gerion, D.; Ding, L.; Elboudwarej, O.; Cooke, P. A.; Gray, J. W.; Alivisatos, A. P.; Chen, F. F. *Nano Lett.* **2006**, *6*, 800–808.
(8) Graf, C.; Vossen, D. L. J.; Imhof, A.; van Blaaderen, A. *Langmuir* **2003**, *19*, 6693–6700.
(9) Mulvaney, P.; Liz-Marzán, L. M.; Giersig, M.; Ung, T. *J. Mater. Chem.* **2000**, *10*, 1259–1270.
(10) Bruchez, M.; Moronne, M.; Gin, P.; Weiss, S.; Alivisatos, A. P. *Science* **1998**, *281*, 2013–2016.
(11) Liz-Marzán, L. M.; Giersig, M.; Mulvaney, P. *Langmuir* **1996**, *12*, 4329–4335.
(12) Zhelev, Z.; Ohba, H.; Bakalova, R. *J. Am. Chem. Soc.* **2006**, *128*, 6324–6325.
(13) Yi, D. K.; Selvan, S. T.; Lee, S. S.; Papaefthymiou, G. C.; Kundaliya, D.; Ying, J. Y *J. Am. Chem. Soc.* **2005**, *127*, 4990–4991.
(14) Wolcott, A.; Gerion, D.; Visconte, M.; Sun, J.; Schwartzberg, A.; Chen, S.; Zhang, J. Z *J. Phys. Chem. B* **2006**, *110*, 5779–5789.
(15) Selvan, S. T.; Patra, P. K.; Ang, C. Y.; Ying, J. Y. *Angew. Chem., Int. Ed.* **2007**, *46*, 2448–2452.
(16) Han, R. C.; Yu, M.; Zheng, Q.; Wang, L. J.; Hong, Y. K.; Sha, Y. L. *Langmuir* **2009**, *25*, 12250–12255.
(17) Daniele, G.; Pinaud, F.; Williams, S. C.; Parak, W. J.; Zanchet, D.; Weiss, S.; Alivisatos, A. P. *J. Phys. Chem. B* **2001**, *105*, 8861–8871.
(18) Rogach, A. L.; Nagesha, D.; Ostrander, J. W.; Giersig, M.; Kotov, N. A. *Chem. Mater.* **2000**, *12*, 2676–2685.
(19) Yang, P.; Ando, M.; Murase, N. *New J. Chem.* **2009**, *33*, 561–567.
(20) Paniğrahi, S.; Bera, A.; Basak, D. *ACS Appl. Mater. Interfaces* **2009**, *1*, 2408–2411.
(21) Stöber, W.; Fink, A.; Bohn, E. *J. Colloid Interface Sci.* **1968**, *26*, 62–66.
(22) Nann, T.; Mulvaney, P. *Angew. Chem., Int. Ed.* **2004**, *43*, 5393–5396.
(23) Yang, P.; Ando, M.; Murase, N. *J. Colloid Interface Sci.* **2007**, *316*, 420–427.
(24) Correa-Duarte, M. A.; Giersig, M.; Liz-Marzán, L. M. *Chem. Phys. Lett.* **1998**, *286*, 497–501.
(25) Koole, R.; van Schooneveld, M. M.; Hilhorst, J.; Donegá, C. M.; Hart, D. C.; van Blaaderen, A.; Vanmaekelbergh, D.; Meijerink, A *Chem. Mater.* **2008**, *20*, 2503–2512.
(26) Yang, Y. H.; Gao, M. Y. *Adv. Mater.* **2005**, *17*, 2354–2357.
(27) Selvan, S. T.; Tan, T. T.; Ying, J. Y. *Adv. Mater.* **2005**, *17*, 1620–1625.
(28) Darbandi, M.; Thomann, R.; Nann, T. *Chem. Mater.* **2005**, *17*, 5720–5725.
(29) Yang, Y. H.; Jing, L. H.; Yu, X. L.; Yan, D. D.; Gao, M. Y. *Chem. Mater.* **2007**, *19*, 4123–4128.
(30) Lai, C. W.; Wang, Y. H.; Chen, Y. C.; Hsieh, C. C.; Uttam, B. P.; Hsiao, J. K.; Hsu, C. C.; Chou, P. T. *J. Mater. Chem.* **2009**, *19*, 8314–8319.
(31) Dong, B. H.; Gao, L. X.; Su, G.; Liu, W.; Qu, H.; Jiang, D. X. *J. Colloid Interface Sci.* **2009**, *339*, 78–82.
(32) Zhou, L.; Gao, C.; Xu, W. J.; Wang, X.; Xu, Y. H. *Biomacromolecules* **2009**, *10*, 1865–1874.
(33) Gaponik, N.; Talapin, D. V.; Rogach, A. L.; Hoppe, K.; Shevchenko, E. V.; Kornowski, A.; Eychmu1ller, A.; Weller, H. *J. Phys. Chem. B* **2002**, *106*, 7177–7185.
(34) Qian, H. F.; Dong, C. Q.; Weng, J. F.; Ren, J. C. *Small* **2006**, *2*, 747–751.
(35) Zhang, H.; Wang, D. Y.; Yang, B.; Möhwald, H. *J. Am. Chem. Soc.* **2006**, *128*, 10171–10180.
(36) Yu, W. W.; Qu, L. H.; Guo, W. Z.; Peng, X. G. *Chem. Mater.* **2003**, *15*, 2854–2860.
(37) Ge, J. P.; Xu, S.; Zhuang, J.; Wang, X.; Peng, Q.; Li, Y. D. *Inorg. Chem.* **2006**, *45*, 4922–4927.
(38) Tekin, E.; Smith, P. J.; Hoeppener, S.; van den Berg, A. M. J.; Susha, A. S.; Rogach, A. L.; Feldmann, J.; Schubert, U. S. *Adv. Funct. Mater.* **2007**, *17*, 23–28.
(39) Kirchner, C.; Liedl, T.; Kudera, S.; Pellegrino, T.; Javier, A. M.; Gaub, H. E.; Stölzle, S.; Fertig, N.; Parak, W. J. *Nano Lett.* **2005**, *5*, 331–338.
(40) Seo, H.; Kim, S. W. *Chem. Mater.* **2007**, *19*, 2715–2717.
(41) Schreder, B.; Schmidt, T.; Ptatschek, V.; Winkler, U.; Materny, A.; Umbach, E.; Lerch, M.; Mü1ller, G.; Kiefer, W.; Spanhel, L. *J. Phys. Chem. B* **2000**, *104*, 1677–1685.
(42) Zhou, L.; Gao, C.; Xu, W. J. *J. Mater. Chem.* **2009**, *19*, 5655–5664.
(43) Bu, J.; Li, R. J.; Quah, C. W.; Carpenter, K. J. *Macromolecules* **2004**, *37*, 6687–6694.

AM9009296